Improving the photostability of bright monomeric orange and red fluorescent proteins

Nathan C Shaner[1,5], Michael Z Lin[1,2], Michael R McKeown[1,2], Paul A Steinbach[1,2], Kristin L Hazelwood[4], Michael W Davidson[4] & Roger Y Tsien[1–3]

All organic fluorophores undergo irreversible photobleaching during prolonged illumination. Although fluorescent proteins typically bleach at a substantially slower rate than many small-molecule dyes, in many cases the lack of sufficient photostability remains an important limiting factor for experiments requiring large numbers of images of single cells. Screening methods focusing solely on brightness or wavelength are highly effective in optimizing both properties, but the absence of selective pressure for photostability in such screens leads to unpredictable photobleaching behavior in the resulting fluorescent proteins. Here we describe an assay for screening libraries of fluorescent proteins for enhanced photostability. With this assay, we developed highly photostable variants of mOrange (a wavelength-shifted monomeric derivative of DsRed from Discosoma sp.) and TagRFP (a monomeric derivative of eqFP578 from Entacmaea quadricolor) that maintain most of the beneficial qualities of the original proteins and perform as reliably as Aequorea victoria GFP derivatives in fusion constructs.

Substantial progress has recently been made in developing monomeric or dimeric fluorescent proteins covering the visual spectrum[1–13], but although brightness and wavelength have been primary concerns, photostability has generally been an afterthought (with the notable exception of mTFP1; ref. 12). Consequently, many new fluorescent protein variants have relatively poor photostability. The first-generation monomeric red fluorescent protein, mRFP1 (ref. 1), although reasonably bright, was less photostable than its ancestor, Discosoma sp. DsRed[14]. In subsequent generations of mRFP1 variants (the 'mFruits'), we observed serendipitous enhancement in photostability in some variants[2], leading us to believe that it would be possible to apply directed evolution strategies to this property as well.

To extend the utility of fluorescent proteins, having optimized them for many other properties, we developed a screening method that additionally assays photostability in a medium-throughput format during directed evolution. Using a high-intensity light source, we photobleached entire 10-cm plates of bacteria expressing the fluorescent proteins of interest and selected those that maintained the most brightness. This approach allowed us to screen libraries containing up to 100,000 clones reliably with no observed false-positive hits and to select simultaneously for the most photostable mutants that also maintained an acceptable level of fluorescence emission at the desired wavelength, minimizing the tradeoff of desirable properties that frequently results from single-parameter screens. We applied our photostability screening assay to the directed evolution of variants derived from the bright red monomeric red fluorescent protein TagRFP and the fast-bleaching monomeric orange fluorescent protein mOrange. The resulting variants, TagRFP-T and mOrange2, were ninefold and 25-fold more photostable than their respective ancestors, and both made excellent fusion partners when expressed in mammalian cells.

RESULTS

Photostability assay and rationale

To photobleach large numbers of bacterial colonies, we used a solar simulator, which produces a collimated beam approximately 10 cm in diameter with light intensities of 95 or 141 mW/cm^2 with 525–555 (540/30) or 548–588 (568/40) nm bandpass filters, respectively. This intensity, although approximately 100-fold lower than that produced by unattenuated arc lamp illumination and 10^5-fold lower than instantaneous intensities during confocal laser illumination, was sufficient to photobleach the photolabile fluorescent protein mOrange to 50% initial intensity after approximately 10 min. This reasonably short time allowed us to quickly screen bacterial libraries of up to 100,000 clones on plates. We minimized the heating of plates by placing them on a custom-built water-cooled aluminum block. At wavelengths necessary to photobleach orange and red fluorescent proteins, we found no substantial decrease in bacterial viability after 2 h of illumination.

Evolution of a brighter photostable red monomer

To create a better red monomer, we initially undertook a rational design approach, drawing on analysis of mCherry's enhanced photostability and mOrange's higher quantum yield relative to mRFP1. Six generations of directed evolution with constant photostability selection yielded the variant 'mApple', which, though

[1]Department of Pharmacology, [2]Howard Hughes Medical Institute and [3]Department of Chemistry and Biochemistry, University of California at San Diego, 9500 Gilman Drive, La Jolla, California 92093, USA. [4]National High Magnetic Field Laboratory and Department of Biological Science, The Florida State University, 1800 East Paul Dirac Drive, Tallahassee, Florida 32310, USA. [5]Present address: The Salk Institute for Biological Studies, 10010 N. Torrey Pines Rd., La Jolla, California 92037, USA. Correspondence should be addressed to R.Y.T. (rtsien@ucsd.edu).

RECEIVED 21 NOVEMBER 2007; ACCEPTED 1 APRIL 2008; PUBLISHED ONLINE 4 MAY 2008; DOI:10.1038/NMETH.1209

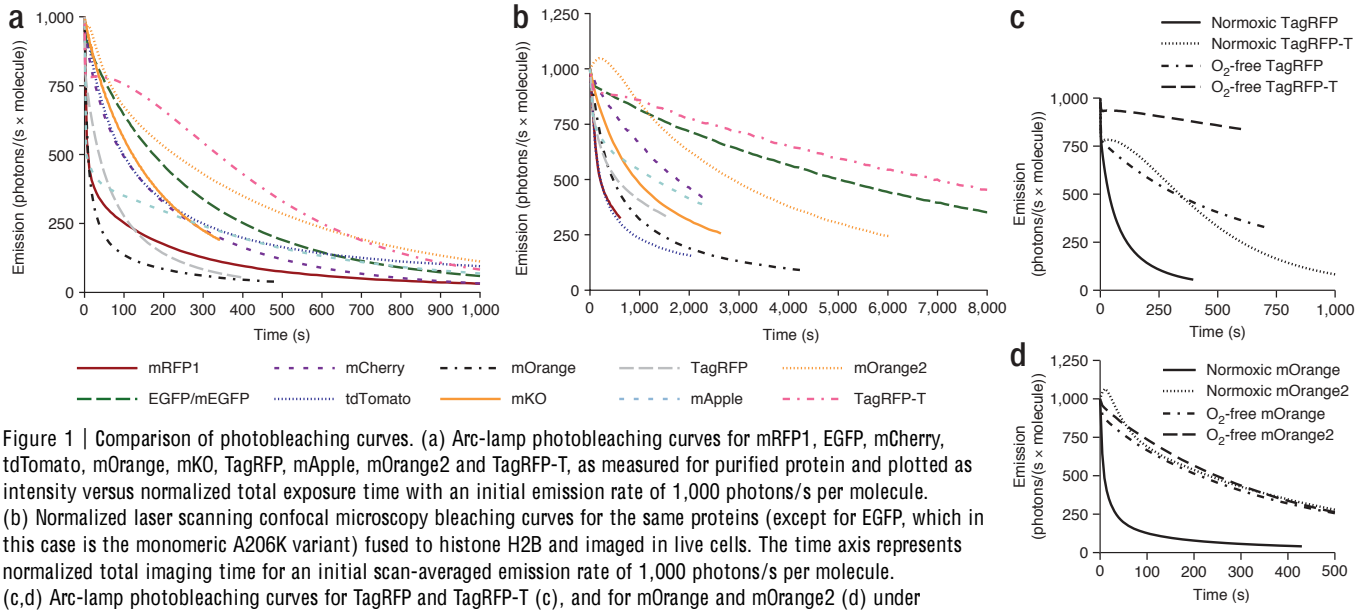

Figure 1 | Comparison of photobleaching curves. (a) Arc-lamp photobleaching curves for mRFP1, EGFP, mCherry, tdTomato, mOrange, mKO, TagRFP, mApple, mOrange2 and TagRFP-T, as measured for purified protein and plotted as intensity versus normalized total exposure time with an initial emission rate of 1,000 photons/s per molecule. (b) Normalized laser scanning confocal microscopy bleaching curves for the same proteins (except for EGFP, which in this case is the monomeric A206K variant) fused to histone H2B and imaged in live cells. The time axis represents normalized total imaging time for an initial scan-averaged emission rate of 1,000 photons/s per molecule. (c,d) Arc-lamp photobleaching curves for TagRFP and TagRFP-T (c), and for mOrange and mOrange2 (d) under normoxic and O_2-free conditions (normalized as in a).

substantially brighter than mCherry, displayed complex photoswitching behavior (Fig. 1 and Tables 1 and 2, and Supplementary Fig. 1 and Supplementary Note 1 online). This behavior was more pronounced with continuous wide-field than with laser-scanning illumination and could be largely eliminated by excitation at alternate wavelengths or by intermittent illumination. However, given our later results using the brighter TagRFP as starting material, we chose not to pursue mApple any further.

Although the recently developed orange-red monomer TagRFP[13] exhibits remarkable brightness, we have found that its photostability is still far from optimal. In both our standard arc-lamp photobleaching and laser-scanning confocal assays, we determined that TagRFP bleaches approximately threefold faster than mCherry (Fig. 1a,b and Table 1). Thus, we chose this protein as another starting point for improvement of photostability. We first attempted rational design of a mutant library guided by the crystal structure of the closely-related protein eqFP611 (ref. 15). With the rationale that chromophore-interacting residues could influence photostability, we performed saturation mutagenesis of Ser158 and Leu199, two residues proximal to the TagRFP chromophore. We then screened this library in bacteria with our solar simulator–based assay, using the 540/30 nm bandpass filter and exposure times of 120 min per plate, imaging the plates before and after bleaching to select those colonies that displayed high absolute brightness and a high ratio of post-bleach to pre-bleach fluorescence emission.

From this directed library, we identified one clone, TagRFP S158T (designated TagRFP-T), which had a photobleaching half-time of 337 s by our standard assay, making it approximately ninefold more photostable than TagRFP (Fig. 1a–c and Table 1). TagRFP-T, which we further modified by appending GFP-like N and C termini, possesses identical excitation and emission

Table 1 | Physical and optical properties of new photostable fluorescent protein variants

Fluorescent protein	Excitation maximum (nm)	Emission maximum (nm)	Extinction coefficient (M^{-1} cm^{-1})	Fluorescence quantum yield	Brightness[a]	pK_a	$t_{1/2}$ for maturation at 37 ıC	$t_{1/2}$ bleach (arc lamp)[b] (s)	$t_{1/2}$ bleach (O_2-free)[c] (s)	$t_{1/2}$ bleach (confocal)[d] (s)
mRFP1	584	607	50,000	0.25	13	4.5	o 1 h	8.7	ND[e]	210
mCherry	587	610	72,000	0.22	16	o 4.5	15 min	96	ND	1,800
mOrange	548	562	71,000	0.69	49	6.5	2.5 h	9.0	250	460
DsRed	558	583	75,000	0.79	59	4.7	10 h	326	ND	ND
tdTomato	554	581	138,000	0.69	95	4.7	60 min	98	ND	210
mKO	548	559	51,600	0.60	31	5.0	4.5 h	122	ND	930
TagRFP[f]	555	584	98,000	0.41	40	3.1	100 min	37	323	550
EGFP or mEGFP	488	507	56,000	0.60	34	6.0	ND	174	ND	5,000
mOrange2	549	565	58,000	0.60	35	6.5	4.5 h	228	228	2,900
mApple	568	592	75,000	0.49	37	6.5	30 min	4.8	ND	1,300
TagRFP-T	555	584	81,000	0.41	33	4.6	100 min	337	4 4600	6,900

[a]Brightness of fully mature protein, (extinction coefficient quantum yield)/1,000. [b]Time to bleach to 50% emission intensity under arc-lamp illumination, at an illumination level that causes each molecule to emit 1,000 photons/s initially, as measured in our lab. See reference 16 for details. [c]With arc lamp illumination, equilibrated under O_2-free conditions. [d]Time to bleach to 50% emission intensity measured during laser scanning confocal microscopy, at an average illumination level over the scanned area that causes each molecule to emit an average 1,000 photons/s initially, as measured in our lab. A 543-nm laser line was used for all proteins except mEGFP, which was bleached with a 488-nm laser (see Supplementary Methods for detailed description of normalization). [e]ND, not determined. [f]All measurements were performed in our lab.

Table 2 | Mutations of new photostable fluorescent protein variants

Protein	Mutations
mApple	mOrange R17H,G40A,T66M,A71V,V73I,K92R,V104I,V105I,T106H, T108N,E117V,S147E,G159S,M163K,T174A,S175A,G196D,T202V
mOrange2	mOrange Q64H,F99Y,E160K,G196D
TagRFP-T	TagRFP S158T

wavelengths, quantum yield and maturation time to TagRFP, with only a slightly lower extinction coefficient (81,000 versus 98,000 M^{-1} cm^{-1}) and a higher fluorescence pK_a, the pH value at which the fluorescent protein exhibits half-maximal fluorescence emission (4.6 versus 3.1). We expect that the benefit of increased photostability should offset the small decrease in brightness and increase in acid sensitivity in most applications. Additionally, TagRFP-T matures to apparent completion and has virtually no emission in the green region of the spectrum (Supplementary Fig. 1), making it suitable for co-imaging with green fluorescent proteins. We verified that TagRFP-T remains monomeric by gel filtration (data not shown). Because the S158T mutation is in the interior of the folded protein, we anticipated that TagRFP-T would perform nearly identically to TagRFP when used as a fusion tag. Indeed, live-cell imaging confirmed that TagRFP-T does not interfere with localization of any fusions tested (Fig. 2).

Photobleaching of TagRFP and TagRFP-T under oxygen-free conditions revealed that TagRFP-T's photobleaching remains oxygen-sensitive (Fig. 1c and Table 1). However, the oxygen-free bleaching half-time for TagRFP is similar to the ambient oxygen bleaching half-time for TagRFP-T. We next compared TagRFP and TagRFP-T as fusions to histone H2B expressed in living cells under confocal illumination (Fig. 1b and Table 1). TagRFP-T had a photobleaching half-time approximately ninefold greater than that of TagRFP, consistent with the results obtained for purified proteins under continuous wide-field illumination.

Evolution of a photostable orange monomer

We next attempted to engineer a photostable variant of mOrange, which is the brightest of the previously engineered mRFP1 variants but exhibits relatively fast bleaching. Because substitutions at position 163 improved photostability during the evolution of mCherry and mApple, we initially tested the M163Q mutant of mOrange, but found that improved photostability was accompanied by undesirable decreases in quantum yield and maturation efficiency. The M163K mutant of mOrange exhibited enhanced photostability and matured very efficiently, but suffered from increased acid sensitivity (pK_a of ~7.5). Because another orange fluorescent protein, mKO (derived from *Fungia concinna*)[6], is both highly photostable[16] and possesses a methionine at the position equivalent to 163, we reasoned that other pathways must exist for increasing photostability.

To explore alternative photostability-enhancement evolution pathways, we used iterative random and directed mutagenesis and selection using the solar simulator. Initially we screened a randomly mutagenized library of mOrange by photobleaching with 540/30 nm light for 15–20 min per plate (a time sufficient to bleach mOrange to ~25% of its initial brightness) and selecting the brightest post-bleach clones by eye. This screen identified a single

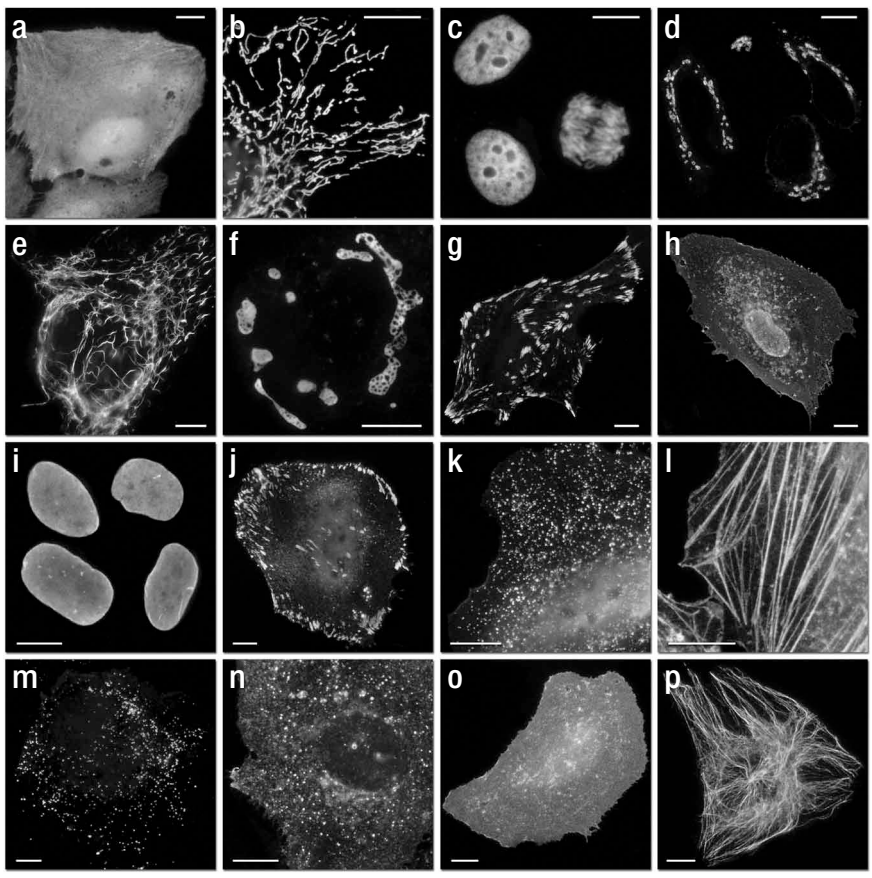

Figure 2 | Fluorescence imaging of TagRFP-T subcellular targeting fusions. (a–g) N-terminal fusion constructs (linker amino acid length indicated by the numbers): TagRFP-T–N1 (a; N-terminal fusion cloning vector; expression in nucleus and cytoplasm with no specific localization); TagRFP-T–7–cytochrome c oxidase (b; mitochondria human cytochrome c oxidase subunit VIII); TagRFP-T–6–histone H2B (c; human; showing two interphase nuclei and one nucleus in early anaphase); TagRFP-T–7–b-1,4-galactosyltransferase (d; golgi; N-terminal 81 amino acids of human b-1,4-galactosyltransferase); TagRFP-T–7-vimentin (e; human); TagRFP-T–7-Cx43 (f; rat a-1 connexin-43); and TagRFP-T–7-zyxin (g; human). (h–p) C-terminal fusion constructs (linker amino acid length indicated by the numbers): annexin (A4)–12–TagRFP-T (h; human; illustrated with ionomycin-induced translocation to the plasma and nuclear membranes); lamin B1–10–TagRFP-T (i; human); vinculin-23–TagRFP-T (j; human); clathrin light chain–15–TagRFP-T (k; human); b-actin–7–TagRFP-T (l; human); PTS1-2–TagRFP-T (m; peroximal targeting signal 1); RhoB-15–TagRFP-T (n; human RhoB GTPase with an N-terminal c-Myc epitope tag; endosome targeting); farnesyl-5–TagRFP-T (o; 20-amino-acid farnesylation signal from c-Ha-Ras); and b-tubulin–6–TagRFP-T (p; human). All TagRFP-T fusion vectors were expressed in HeLa (CCL-2) cells. Scale bars, 10 mm.

clone, mOrange F99Y, which had approximately twofold improved photostability (data not shown). Saturation mutagenesis of residue 99—and residues 97 and 163, which we imagined could have synergistic interactions with residue 99—did not yield additional improvements.

We then constructed a randomly mutagenized library of mOrange F99Y and screened with a longer illumination time of 40 min per plate. This round of screening identified an additional mutation, Q64H, which conferred about a tenfold increase in photostability over the mOrange F99Y single mutant. Again, saturation mutagenesis of residues 64 and 99 along with neighboring residues 97 and 163 did not produce clones that were improved over the original clone identified in the random screen. Additionally, we found that the Q64H mutation alone did not confer substantially enhanced photostability but required the presence of the F99Y mutation (data not shown). Two additional rounds of directed evolution with continued selection for photostability (540/30 nm filter, 40 min per plate) improved the folding efficiency with mutations E160K and G196D, giving the final clone, mOrange2 (Table 2).

The highly desirable increase in photostability achieved in mOrange2 is balanced by a modest decrease in quantum yield (0.60 versus 0.69) and extinction coefficient (58,000 versus 72,000 M^{-1} cm^{-1}), together corresponding to a 30% decrease in brightness compared to mOrange. It also exhibits slightly shifted excitation and emission peaks (549 nm and 565 nm) and an increased maturation half-time (4.5 h versus 2.5 h; Table 1). However, its photostability under arc-lamp illumination is over 25-fold greater than that of mOrange (Fig. 1d), making it nearly twice as photostable as mKO[6], the previously most photostable known orange monomer[16], approximately sixfold more photostable than TagRFP[13] and about 1.3-fold more photostable than enhanced GFP (EGFP)[16] (Fig. 1 and Table 2). During laser-scanning confocal imaging, mOrange2 was approximately sixfold more photostable than mOrange and threefold more photostable than mKO (Fig. 1b). Notably, the brightness and maturation time of mOrange2 are quite similar to those for mKO. mOrange2 remains acid-sensitive with a pK_a of 6.5, making it undesirable for targeting to acidic compartments, but attractive as a possible marker for exocytosis or other pH-variable processes[17]. Also, because it contains a small fraction of immature (but nonfluorescent) chromophore (Supplementary Fig. 1), mOrange2 may not be an ideal FRET acceptor. As with TagRFP-T, we verified that mOrange2 remained monomeric using gel filtration (data not shown). We then investigated the role of the key photostability-enhancing mutations present in mOrange2, tested it in a wide range of fusion constructs, and compared its performance with that of mKO and tdTomato (Fig. 3 and Supplementary Note 2 online).

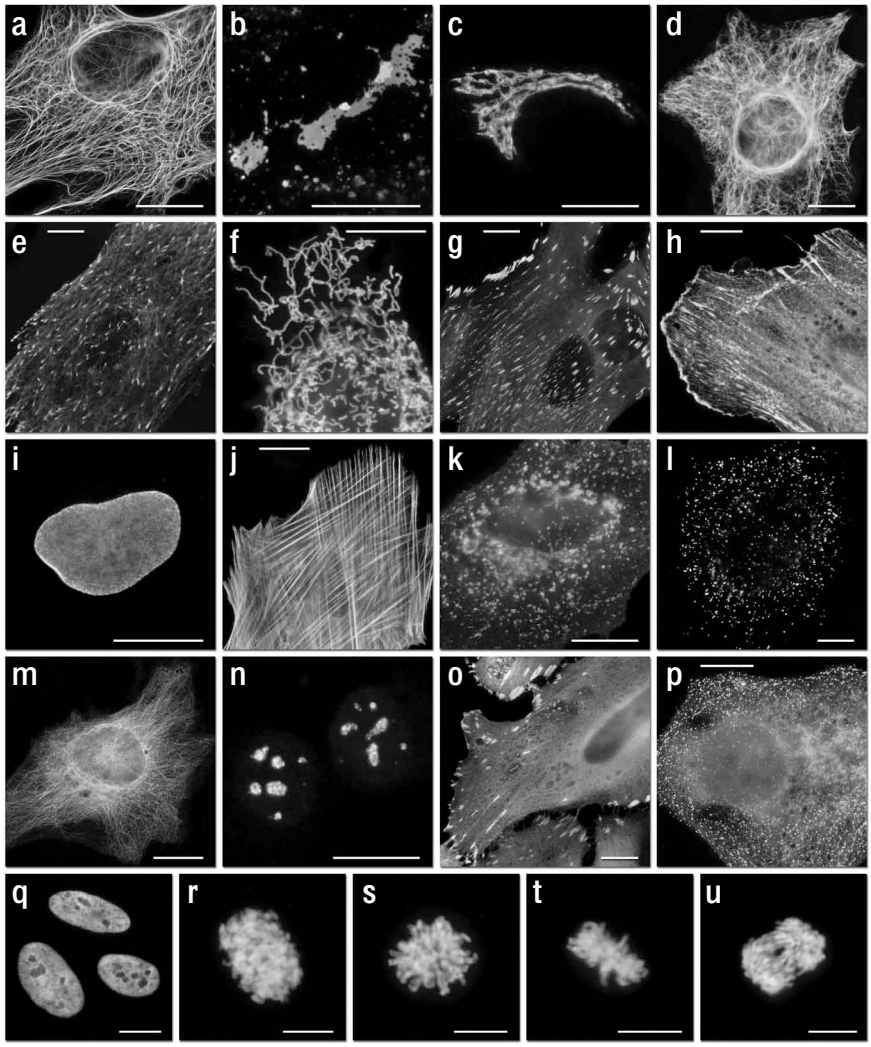

Figure 3 | Widefield fluorescence imaging of mOrange2 subcellular targeting fusions. (a–h) N-terminal fusion constructs (linker amino acid length indicated by the numbers): mOrange2-17-keratin (a; human cytokeratin 18); mOrange2-7-Cx26 (b; rat b-2 connexin-26); mOrange2-7–b-1,4-galactosyltransferase (c; golgi; N-terminal 81 amino acids of human b-1,4-galactosyltransferase); mOrange2-7-vimentin (d; human); mOrange2-7-EB3 (e; human microtubule-associated protein; RP/EB family); mOrange2-7–cytochrome c oxidase (f; mitochondria; human cytochrome c oxidase subunit VIII); mOrange2-22-paxillin (g; chicken); and mOrange2-19–a-actinin (h; human non-muscle). (i–p) C-terminal fusion constructs (linker amino acid length indicated by the numbers): lamin B1–10-mOrange2 (i; human); b-actin–7-mOrange2 (j; human); glycoprotein 1–20-mOrange2 (k; rat lysosomal membrane glycoprotein 1); peroxisomal targeting signal 1–2-mOrange2 (l); b-tubulin–6-mOrange2 (m; human); fibrillarin-7-mOrange2 (n; human); vinculin-23-mOrange2 (o; human); and clathrin light chain-15-mOrange2 (p; human). (q–u) Laser scanning confocal images of HeLa cells expressing histone H2B–6-mOrange2 (N-terminal fusion; human) progressing through interphase (q), prophase (r), prometaphase (s), metaphase (t) and early anaphase (u). The cell line used for expressing mOrange2 fusion vectors was Gray fox lung fibroblast cells (FoLu) in e and j, and human cervical adenocarcinoma cells (HeLa) in the remaining panels. Scale bars, 10 mm.

Evaluation of reversible photoswitching

Because of concerns that our screening method might select for photoswitching behavior, we tested our selected variants as well as other commonly used fluorescent proteins using both widefield and confocal imaging. Nearly all had some degree of reversible photoswitching, which we observed as a recovery of up to 100% of pre-bleach fluorescence intensity when the fluorescent protein was bleached to ~50% of its initial intensity and then observed again after 1–2 min without illumination. In fact, several commonly used *A. victoria* GFP variants including EGFP, Cerulean and Venus, displayed reversible photoswitching[18] more severe than that observed for the variants we identified. A summary table of the results of these experiments along with representative traces for TagRFP, TagRFP-T, EGFP and Cerulean are available in Supplementary Note 3 online. These results suggest that our screen is not selecting specifically for photoswitching, which is no worse in the new proteins (except for mApple) than in well-established fluorescent proteins.

Although our observation of reversible photoswitching in such a broad range of fluorescent proteins certainly raises concerns about the potential for previously undetected experimental artifacts, it is beyond the scope of this study to determine how common or severe this phenomenon may be. Of particular concern is the implication that fluorescence recovery after photobleaching experiments may be prone to artifacts that would confound data interpretation. We performed a limited evaluation of this possibility using histone H2B fusions to EGFP and EYFP expressed in mammalian cells and imaged on a laser-scanning confocal microscope. When we bleached these proteins to near completion with full laser power and then observed for recovery, we observed a negligible amount of reversible photoswitching (data not shown). However, an in-depth investigation is warranted to rule out such an effect in other fluorescent proteins and under more varied experimental conditions.

DISCUSSION

Although the precise kinetics of photobleaching for a given fluorescent protein are strongly dependent on illumination intensity and temporal regimen, we found that improvements in photostability at ~0.1 W/cm^2 usually qualitatively predict improved performance under typical conditions for wide-field and laser scanning microscopy. The exceptions were mApple's reversible photoswitching (Supplementary Note 1) and tdTomato's poor performance under laser scanning confocal illumination (Fig. 1b). Also, our screen used bacteria to express fluorescent protein libraries, but all proteins produced from these studies behaved similarly when later tested in purified form or expressed in mammalian cells, consistent with our previous experience.

Fluorescent proteins had been photobleached using an array of LEDs during the evolution of mTFP1 to select against unacceptable photolability or photoswitching, resulting in a protein with a bleaching half-time 110 s[12]. We applied photostability as a primary criterion to improve multiple fluorescent proteins, and our results demonstrate that high photostability is a selectable phenotype. Moreover, a solar simulator takes advantage of the strong mercury lines at 546, 577 and 579 nm and allows greater flexibility in the choice of excitation wavelength than would be possible with LEDs.

Although it is difficult to draw strong conclusions about exact mechanisms of photobleaching from the mutations that confer photostability to mOrange2, specific regions proximal to the chromophore appear to influence the modes of photobleaching the protein is able to undergo. DsRed, when illuminated by a 532-nm pulsed laser, undergoes decarboxylation of Glu215, as well as *cis*-to-*trans* isomerization of the chromophore[19]. Such chromophore isomerization has been implicated in the photoswitching behavior of Kindling fluorescent protein (KFP)[20,21] and Dronpa[5,22] as well as predecessors to mTFP1 (refs. 12 and 23). Decarboxylation of the corresponding glutamate (position 222) in *A. victoria* GFP also leads to changes in optical properties[24–26]. However, our observation that oxidation is important in mOrange, TagRFP and TagRFP-T photobleaching suggests that chromophore isomerization and Glu215 decarboxylation may have only a minor role for such proteins under normoxic conditions. Additionally, we found no evidence by mass spectrometry that photobleaching using the solar simulator led to any detectable decarboxylation of Glu215 in mOrange (data not shown). Under some conditions mOrange2 shows an initial photoactivation of about 5% (Fig. 1a,d) before bleaching takes over. At present we have no molecular explanation for this effect or the reversible photoswitching that is common to most fluorescent proteins (Supplementary Note 3).

For mRFP1 variants, we observed the importance of residue 163 in influencing photostability (Supplementary Note 1) but also observed somewhat context-specific effects of residue 163 and surrounding residues on different wavelength-shifted variants. This region, composed of residues 64, 97, 99 and 163, appears to be important in determining photostability. However, of these, only residue 163 is in direct contact with the chromophore. It may be that the mutations Q64H and F99Y together lead to a rearrangement of the other side chains in the vicinity of the chromophore so as to hinder a critical oxidation that leads to loss of fluorescence.

Discrepancies in tubulin and connexin localization (Supplementary Note 2) when fused to mOrange2 versus mKO or tdTomato can probably be attributed to the three-dimensional structure of the fluorescent protein and potential steric hindrance in the fusions. mOrange2 contains extended N and C termini derived from EGFP to improve performance in fusions, whereas the much shorter protein, mKO (218 versus 236 amino acids), may experience steric interferences that lead to poorer performance in similar fusions. The fused dimeric character of tdTomato effectively doubles its size compared to the monomeric orange fluorescent proteins, so steric hindrance is the most likely culprit in preventing tubulin localization. For most fusions, however, we observed little or no difference in performance between mOrange2 and mKO, suggesting that many proteins are more tolerant of fusion partners than tubulin or connexins.

Though it already possessed reasonably good photostability, TagRFP was still amenable to improvements by our photostability selection method. From a saturation-mutagenesis library of two chromophore-proximal residues (consisting of 400 independent clones), we selected a single clone with substantially enhanced photostability. The selected mutant, TagRFP-T, should prove to be a very useful addition to the fluorescent protein arsenal, as it is the most photostable monomeric fluorescent protein of any color yet described under both arc-lamp and confocal laser illumination.

As the applications of genetically encoded fluorescent markers continue to diversify and become more complex, the demand for greater photostability than is now available in fluorescent proteins has likewise continued to grow. We expect our screening method to

be applicable to any of the existing fluorescent proteins and, with modifications, to be useful in selecting for more efficient photoconvertible and photoswitchable fluorescent proteins as well[3,5,10,20,27–31]. Possible enhancements to this selection technique could include time-lapse imaging of bacterial plates during bleaching to enable direct selection for kinetics (independent of absolute brightness) and the use of higher-intensity illumination from other light sources (such as lasers) during screening to select for or against nonlinear photobleaching behavior. Ideally, a selection scheme that allows true simulation of microscopic imaging light intensities while maintaining a medium-to-high throughput should allow selection of fluorescent proteins with the most beneficial properties for imaging applications.

METHODS

Mutagenesis. As the initial templates for library construction by random mutagenesis we used cDNA encoding mOrange[2] and TagRFP (Evrogen)[13], both of which had been previously human codon–optimized. We performed error-prone PCR using the GeneMorph II kit (Stratagene) following the manufacturer's protocol, using primers containing BamHI and EcoRI sites for mOrange variants or BamHI and BsrGI sites for TagRFP variants. We digested products of error-prone PCR products with appropriate restriction enzymes and ligated the fragments into a modified pBAD vector (Invitrogen) or a constitutive bacterial expression vector pNCS, both of which encode an N-terminal 6His tag and linker identical to that found in pRSET B (Invitrogen). We performed site-directed mutagenesis using the QuikChange II kit (Stratagene) following the manufacturer's protocol or by overlap-extension PCR. Sequences for all primers used in this study are available in Supplementary Methods online. We transformed chemically competent or electrocompetent Escherichia coli strain LMG194 (Invitrogen) cells with libraries and grew them overnight at 37 1C on LB-agar supplemented with 50 mg/ml ampicillin (Sigma) and 0.02% (wt/vol) L-arabinose (Fluka) (for pBAD-based libraries).

Library screening. For each round of random mutagenesis, we screened 20,000–100,000 colonies (10–50 plates of bacteria), a number sufficient to sample all possible single-site mutants and a limited number of double mutants. For each round of site-directed mutagenesis, we screened approximately threefold more colonies than the expected library diversity (for example, 1,200 colonies for a 400-member library) to ensure full coverage. We photobleached whole plates of bacteria for 10–120 min (determined empirically for each round of directed evolution) on a Spectra-Physics 92191–1000 solar simulator with a 1,600 W mercury arc lamp equipped with two Spectra-Physics SP66239-3767 dichroic mirrors to remove infrared and ultraviolet wavelengths. Remaining light was filtered through 10-cm square bandpass filters (Chroma Technology Corp.) appropriate to the fluorescent protein being bleached (540/30 nm (B540/30; 525–555 nm) for mOrange- and TagRFP-based libraries or 568/40 nm (B568/40; 548–588 nm) for mApple libraries). We measured final light intensities produced by the solar simulator by a miniature integrating-sphere detector (SPD024 head and ILC1700 meter, International Light Corp.) to be 95 mW/cm^2 for the 540/30 filter and 141 mW/cm^2 for the 568/40 filter. We maintained the temperature of the bacterial plates at 20 1C during solar simulator bleaching using a home-built water-cooled aluminum block. For mOrange mutant selection, we examined the plates by eye as previously described[32] using a 150 W xenon lamp equipped with a 540/30 nm excitation filter and fiber optic light guides to illuminate the plates and 575 nm long pass filter to visualize emission. For TagRFP mutant selection, we imaged the plates before and after bleaching on an imaging system (UVP) using 535/45 nm (512.5–557.5 nm) excitation and 605/70 nm (570–640 nm) emission filters. In either case, we grew colonies that maintained bright fluorescence after photobleaching and/or those with high post- to pre-bleach fluorescence ratios for 8 h in 2 ml of LB medium supplemented with 100 mg/ml ampicillin and then increased the culture volume to 4 ml with additional LB supplemented with ampicillin and 0.2% (wt/vol) L-arabinose to induce fluorescent protein expression and grew the cultures overnight. We extracted protein from a fraction of each cell pellet with B-PER II (Pierce) and obtained spectra using a Safire 96-well plate reader with monochromators (Tecan). When screening for photostable variants, we obtained spectra before and after photobleaching extracted protein on the solar simulator. We extracted plasmid DNA from the remaining cell pellet with a miniprep kit (Qiagen) and used it for sequencing.

Protein production and characterization. We expressed fluorescent proteins from pBAD vectors in E. coli strain LMG194, purified them on Ni-NTA agarose (Qiagen) and characterized them as described[2]. Photobleaching measurements were performed on aqueous droplets of purified protein under oil as described[2,16]. To determine whether the presence of molecular oxygen influenced bleaching, we performed our standard bleaching experiment before and after equilibrating the entire bleaching apparatus under humidified N_2.

Additional methods. Primer list, descriptions of mass spectrometry analysis, mammalian expression vectors, live-cell imaging and laser scanning confocal microscopy live-cell photobleaching are available in Supplementary Methods.

Accession numbers. GenBank: DQ336159 (mOrange2), DQ336160 (mApple) and EU582019 (TagRFP-T).

Note: Supplementary information is available on the Nature Methods website.

ACKNOWLEDGMENTS

L.A. Gross performed mass spectroscopy. S.R. Adams performed gel filtration experiments. We thank R.E. Campbell and C.T. Dooley for helpful discussion. Sequencing services were provided by the University of California, San Diego Cancer Center shared sequencing resource and the Florida State University Bioanalytical and Molecular Cloning DNA Sequencing Laboratory. N.C.S. was a Howard Hughes Medical Institute predoctoral fellow during this work. This work was additionally supported by the US National Institutes of Health (NS27177 and GM72033) and the Howard Hughes Medical Institute.

AUTHOR CONTRIBUTIONS

N.C.S. designed the photostability selection protocol, performed all directed evolution and physical characterization of mApple and mOrange2, analyzed and organized all data collected by other authors, and prepared the manuscript; M.Z.L. and M.R.M. performed directed evolution and physical characterization of TagRFP-T; P.A.S. designed the home-built components of the solar simulator apparatus and performed photobleaching measurements of purified proteins; K.L.H. and M.W.D. constructed mammalian expression vectors and performed all microscopy experiments involving live cells; R.Y.T. contributed to conceptual development, data analysis and manuscript preparation; all authors contributed to editing the manuscript.

COMPETING INTERESTS STATEMENT
The authors declare competing financial interests: details accompany the full-text HTML version of the paper at http://www.nature.com/naturemethods/.

Published online at http://www.nature.com/naturemethods/
Reprints and permissions information is available online at http://npg.nature.com/reprintsandpermissions

1. Campbell, R.E. et al. A monomeric red fluorescent protein. Proc. Natl. Acad. Sci. USA 99, 7877–7882 (2002).
2. Shaner, N.C. et al. Improved monomeric red, orange and yellow fluorescent proteins derived from Discosoma sp. red fluorescent protein. Nat. Biotechnol. 22, 1567–1572 (2004).
3. Chudakov, D.M. et al. Photoswitchable cyan fluorescent protein for protein tracking. Nat. Biotechnol. 22, 1435–1439 (2004).
4. Griesbeck, O., Baird, G.S., Campbell, R.E., Zacharias, D.A. & Tsien, R.Y. Reducing the environmental sensitivity of yellow fluorescent protein. Mechanism and applications. J. Biol. Chem. 276, 29188–29194 (2001).
5. Habuchi, S. et al. Reversible single-molecule photoswitching in the GFP-like fluorescent protein Dronpa. Proc. Natl. Acad. Sci. USA 102, 9511–9516 (2005).
6. Karasawa, S., Araki, T., Nagai, T., Mizuno, H. & Miyawaki, A. Cyan-emitting and orange-emitting fluorescent proteins as a donor/acceptor pair for fluorescence resonance energy transfer. Biochem. J. 381, 307–312 (2004).
7. Nagai, T. et al. A variant of yellow fluorescent protein with fast and efficient maturation for cell-biological applications. Nat. Biotechnol. 20, 87–90 (2002).
8. Nguyen, A.W. & Daugherty, P.S. Evolutionary optimization of fluorescent proteins for intracellular FRET. Nat. Biotechnol. 23, 355–360 (2005).
9. Rizzo, M.A., Springer, G.H., Granada, B. & Piston, D.W. An improved cyan fluorescent protein variant useful for FRET. Nat. Biotechnol. 22, 445–449 (2004).
10. Wiedenmann, J. et al. EosFP, a fluorescent marker protein with UV-inducible green-to-red fluorescence conversion. Proc. Natl. Acad. Sci. USA 101, 15905–15910 (2004).
11. Zapata-Hommer, O. & Griesbeck, O. Efficiently folding and circularly permuted variants of the Sapphire mutant of GFP. BMC Biotechnol. 3, 5 (2003).
12. Ai, H.W., Henderson, J.N., Remington, S.J. & Campbell, R.E. Directed evolution of a monomeric, bright and photostable version of Clavularia cyan fluorescent protein: structural characterization and applications in fluorescence imaging. Biochem. J. 400, 531–540 (2006).
13. Merzlyak, E.M. et al. Bright monomeric red fluorescent protein with an extended fluorescence lifetime. Nat. Methods 4, 555–557 (2007).
14. Matz, M.V. et al. Fluorescent proteins from nonbioluminescent Anthozoa species. Nat. Biotechnol. 17, 969–973 (1999).
15. Petersen, J. et al. The 2.0-A crystal structure of eqFP611, a far red fluorescent protein from the sea anemone Entacmaea quadricolor. J. Biol. Chem. 278, 44626–44631 (2003).
16. Shaner, N.C., Steinbach, P.A. & Tsien, R.Y. A guide to choosing fluorescent proteins. Nat. Methods 2, 905–909 (2005).
17. Miesenbock, G., De Angelis, D.A. & Rothman, J.E. Visualizing secretion and synaptic transmission with pH-sensitive green fluorescent proteins. Nature 394, 192–195 (1998).
18. Sinnecker, D., Voigt, P., Hellwig, N. & Schaefer, M. Reversible photobleaching of enhanced green fluorescent proteins. Biochemistry 44, 7085–7094 (2005).
19. Habuchi, S. et al. Evidence for the isomerization and decarboxylation in the photoconversion of the red fluorescent protein DsRed. J. Am. Chem. Soc. 127, 8977–8984 (2005).
20. Chudakov, D.M., Feofanov, A.V., Mudrik, N.N., Lukyanov, S. & Lukyanov, K.A. Chromophore environment provides clue to "kindling fluorescent protein" riddle. J. Biol. Chem. 278, 7215–7219 (2003).
21. Andresen, M. et al. Structure and mechanism of the reversible photoswitch of a fluorescent protein. Proc. Natl. Acad. Sci. USA 102, 13070–13074 (2005).
22. Andresen, M. et al. Structural basis for reversible photoswitching in Dronpa. Proc. Natl. Acad. Sci. USA 104, 13005–13009 (2007).
23. Henderson, J.N., Ai, H.W., Campbell, R.E. & Remington, S.J. Structural basis for reversible photobleaching of a green fluorescent protein homologue. Proc. Natl. Acad. Sci. USA 104, 6672–6677 (2007).
24. van Thor, J.J., Gensch, T., Hellingwerf, K.J. & Johnson, L.N. Phototransformation of green fluorescent protein with UV and visible light leads to decarboxylation of glutamate 222. Nat. Struct. Biol. 9, 37–41 (2002).
25. Bell, A.F., Stoner-Ma, D., Wachter, R.M. & Tonge, P.J. Light-driven decarboxylation of wild-type green fluorescent protein. J. Am. Chem. Soc. 125, 6919–6926 (2003).
26. van Thor, J.J., Georgiev, G.Y., Towrie, M. & Sage, J.T. Ultrafast and low barrier motions in the photoreactions of the green fluorescent protein. J. Biol. Chem. 280, 33652–33659 (2005).
27. Verkhusha, V.V. & Sorkin, A. Conversion of the monomeric red fluorescent protein into a photoactivatable probe. Chem. Biol. 12, 279–285 (2005).
28. Ando, R., Hama, H., Yamamoto-Hino, M., Mizuno, H. & Miyawaki, A. An optical marker based on the UV-induced green-to-red photoconversion of a fluorescent protein. Proc. Natl. Acad. Sci. USA 99, 12651–12656 (2002).
29. Lukyanov, K.A., Chudakov, D.M., Lukyanov, S. & Verkhusha, V.V. Innovation: Photoactivatable fluorescent proteins. Nat. Rev. Mol. Cell Biol. 6, 885–891 (2005).
30. Patterson, G.H. & Lippincott-Schwartz, J. Selective photolabeling of proteins using photoactivatable GFP. Methods 32, 445–450 (2004).
31. Tsutsui, H., Karasawa, S., Shimizu, H., Nukina, N. & Miyawaki, A. Semi-rational engineering of a coral fluorescent protein into an efficient highlighter. EMBO Rep. 6, 233–238 (2005).
32. Baird, G.S., Zacharias, D.A. & Tsien, R.Y. Circular permutation and receptor insertion within green fluorescent proteins. Proc. Natl. Acad. Sci. USA 96, 11241–11246 (1999).

Improving the photostability of bright monomeric orange and red fluorescent proteins

Nathan C Shaner, Michael Z Lin, Michael R McKeown, Paul A Steinbach,

Kristin L Hazelwood, Michael W Davidson & Roger Y Tsien

Supplementary figures and text:

Supplementary Figure 1 Excitation, emission, and absorbance spectra of novel fluorescent protein variants.

Supplementary Note 1 Directed evolution and characterization of mApple.

Supplementary Note 2 Directed evolution and characterization of mOrange2.

Supplementary Note 3 Summary of reversible photoswitching data with representative examples.

Supplementary Methods

Supplementary Figure 1. Excitation, emission, and absorbance spectra of novel fluorescent protein variants.

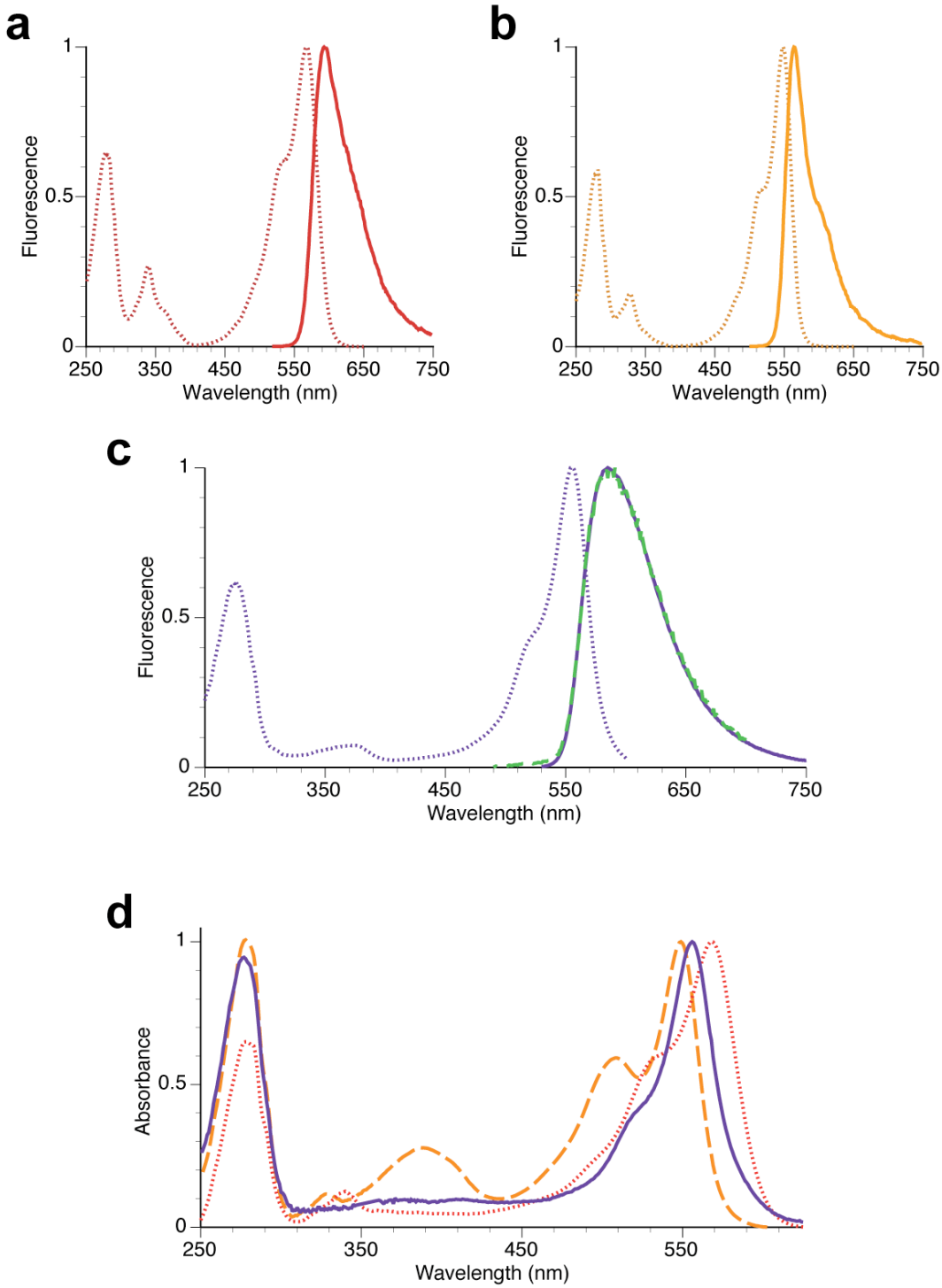

Excitation (measured at emission maximum, solid lines) and emission (measured at excitation maximum, dotted lines) spectra for (**a**) mApple and (**b**) mOrange2, and (**c**) excitation (measured at emission maximum, dotted line) and emission (measured at excitation maximum, purple solid line; measured with 480 nm excitation, green dashed line) spectra for TagRFP-T; (**d**) absorbance spectra for mApple (red dotted line), mOrange2 (orange dashed line) and TagRFP-T (purple solid line).

Supplementary Note 1

Evolution of a brighter photostable red monomer. We began our attempts to create photostable mRFP1-derived fluorescent proteins with an analysis of the most photostable existing variant, mCherry[1]. mCherry exhibits very similar excitation and emission spectra to mRFP1, but has improved maturation efficiency and over 10-fold greater photostability as judged by photon dose required for 50% bleaching. By gathering photobleaching curves for intermediate mutants produced during mCherry directed evolution, we determined that the M163Q mutation present in mCherry was wholly responsible for its increased photostability (data not shown). Residue 163 sits immediately adjacent to the chromophore phenolate, and is occupied by a lysine in wild-type DsRed that forms a salt bridge with the chromophore[2].

We first attempted to simultaneously evolve a brighter and more photostable red fluorescent monomer. The relatively photostable variant mCherry exhibits red fluorescence (ex. 587 nm, em. 610 nm) with a pKa of < 4.5 and a quantum yield of 0.22. However, we observed that at very high pH this variant undergoes a transition to a higher-quantum yield (~0.50) blue-shifted (ex. 568 nm, em. 592 nm) form with a pKa of about 9.5. Since a similar pH-dependence was observed in the early stages of the evolution of mOrange[1], we reasoned that restoring threonine 66 in the chromophore of mOrange to the wild-type glutamine, as in DsRed, (thus restoring red fluorescence) might allow us to find a high-quantum yield red fluorescent variant with a pKa in a practical range.

As predicted, the mOrange T66Q mutant exhibited red fluorescence similar to mCherry, but with a pKa for transition to high-quantum yield red fluorescence at a lower value than mCherry (around 8.0) (data not shown). One round of directed evolution led to the first low-pKa bright red mutant, mApple0.1 (mOrange G40A, T66Q), which had a pKa of 6.4. This mutant, however, exhibited rapid photobleaching (data not shown) and had a substantial fraction of "dead-end" green chromophore[3] which was brightly fluorescent. Subsequent rounds of directed evolution led to the introduction of the mutation M163K, which simultaneously increased photostability markedly and led to almost complete red chromophore maturation. With each round of directed evolution, we included both photostability screening (with irradiation for 20 to 30 minutes per plate using a 568/40 nm bandpass filter) and brightness screening, so this increase of photostability was maintained with each generation.

After 6 rounds of directed evolution, our final variant, mApple, possesses 18 mutations relative to mOrange and 19 mutations relative to mCherry. With a quantum yield of 0.49 and extinction coefficient of 75,000 $M^{-1} \times cm^{-1}$, mApple is more than twice as bright as mCherry. Its reasonably fast maturation time of approximately 30 minutes should

additionally allow rapid detection when expressed in cells (see **Supplementary Fig. 1** online and **Tables 1** and **2** in the main text).

When subjected to constant illumination, mApple displays unusual reversible photoswitching behavior. This photoswitching leads to a reduction in fluorescence emission of between 30 and 70% after several seconds of illumination at typical fluorescence microscope intensities of 1 to 10 W/cm^2 (for example, **Fig. 1a** in the main text, a photobleaching curve taken without neutral density filters). For the immediate precursor to mApple, mApple0.5, this decrease in emission reverses fully within 30 seconds when illumination is discontinued, and cycles of photoswitching and full reversal appear to be repeatable over many cycles without substantial irreversible bleaching (see **Fig. A** below).

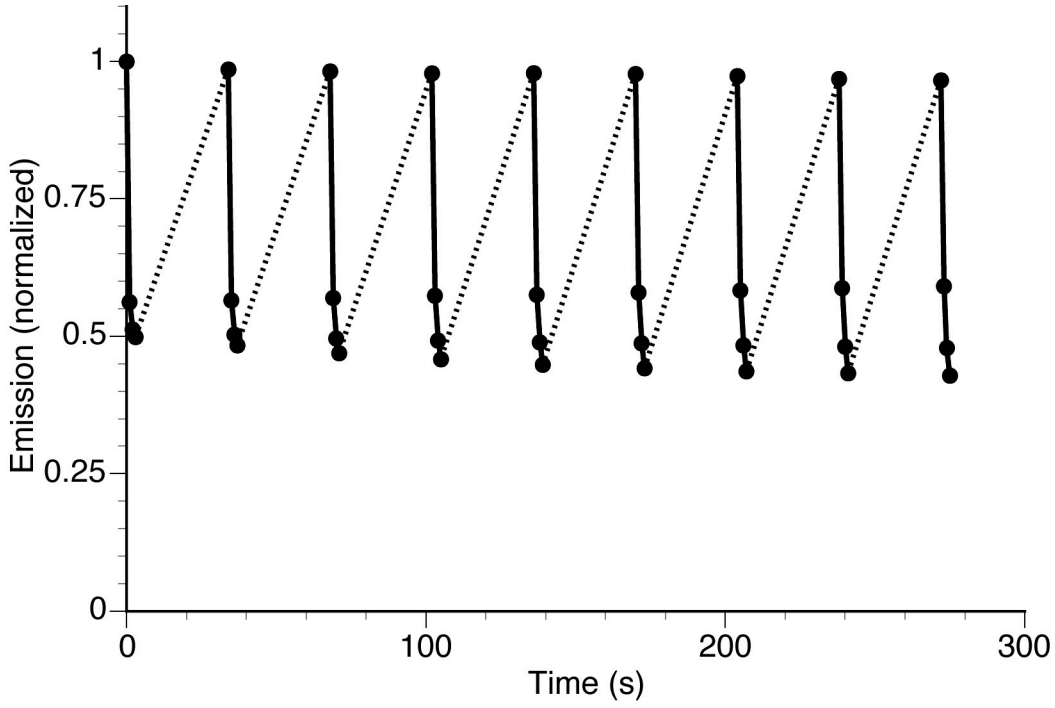

Figure A. Reversible photoswitching in mApple0.5. 10 cycles of continuous arc lamp illumination with 10% neutral density filter for four seconds (solid lines, individual data points shown), with 30 seconds of darkness between cycles (dotted lines) (normalized intensity *versus* actual exposure time). All data points are normalized to the initial image intensity (at time 0); the progressive slight decreases in recovered intensity after each cycle are presumably due to small amounts of irreversible photobleaching or fatigue. mApple0.5 is the immediate precursor to mApple which lacks the external mutations R17H, K92R, S147E, T175A, and T202V.

Because of its photoswitching behavior, mApple displays a short photobleaching $t_{1/2}$ of 4.8 seconds in our standard photobleaching assay (see **Table 1** in the main text). However, mApple appears far more photostable under laser scanning confocal illumination, with a photobleaching $t_{1/2}$ superior to mOrange and mKO, and approaching that of mCherry (see **Table 1** and **Fig. 1b** in the main text). The key difference between the two illumination conditions may be that laser scanning excitation is intermittent for any given pixel, giving time for some recovery in the dark. Also, unless extreme care is taken not to minimize excitation before taking the first image, it is easy to miss the very fast initial phase of decaying emission. All attempts to eliminate mApple's photoswitching behavior by mutagenesis of residues surrounding the chromophore produced unwanted reductions in quantum yield and/or maturation efficiency. However, such photoswitching may make mApple useful for revolutionary new optical techniques for nanoscale spatial resolution ("nanoscopy", see below).

All reversibly photoswitchable fluorescent proteins described thus far operate through *cis*-to-*trans* isomerization of the chromophore[4, 5], so this mechanism is probably responsible for the photoswitching of mApple. The fastest-switching mutant of Dronpa, M159T, relaxes in the dark from its temporarily dark state back to fluorescence with a half-time of 30 sec[6]; mApple is almost completely recovered by 30 sec (**Fig. A**, above), but its behavior is qualitatively similar to Dronpa M159T. Because mApple's spontaneous recovery is already so fast, we have not yet systematically explored acceleration by short-wavelength illumination, but we have noticed that the initial fast decay of emission is absent with 480 nm excitation (**Fig. B**, below), suggesting that this wavelength stimulates recovery from the dark state as well as the primary fluorescence.

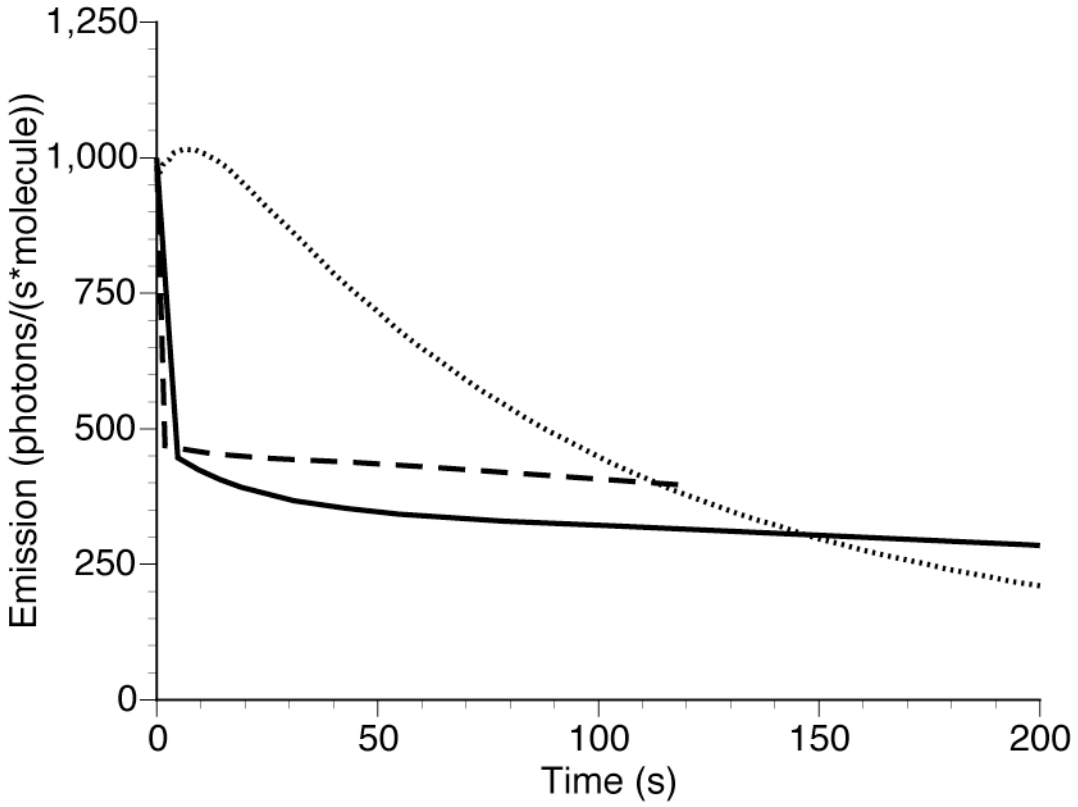

Figure B. mApple photobleaching at different excitation wavelengths. Widefield photobleaching curves for mApple purified protein under oil with excitation using 568/55 nm (solid line), 540/25 nm (dashed line), or 480/30 nm (dotted line) band pass filters, plotted as intensity *versus* normalized total exposure time with an initial emission rate of 1000 photons/s per molecule.

Meanwhile, the existing properties of mApple would seem very attractive for photoactivated localization microscopy with independently running acquisition (PALMIRA[7]). In this exciting new version of super-resolution microscopy, strong illumination (several kW/cm^2) drives most of the fluorophores into a dark state. Individual fluorophores stochastically revert to the fluorescing state, briefly emit a burst of photons, then revert to the dark state. In any one image (whose acquisition time should roughly match the mean duration of an emission burst), the emitters must be sparse enough so that they represent distinct single molecules whose position can be localized to a few nm by centroid-locating algorithms. Superposition of the centroid locations over many images produces a super-resolution composite image. Currently the only genetically encoded, photoreversible fluorophores are Dronpa, asFP595, and their engineered variants. Dronpa fluoresces green and requires an excitation wavelength (488 nm) that slightly stimulates photoactivation of the dark molecules as well as fluorescence and quenching of the bright molecules. asFP595 emits in the red but is very dim (quantum yield <0.001) and tetrameric, whereas mApple also emits red but is quite bright (quantum yield 0.49), very photostable apart from its fast photoswitching, and monomeric. Although **Fig. B** (above) shows photoswitching only down to ~30% of initial

intensity with a few W/cm^2, PALMIRA operates with up to 3 orders of magnitude higher intensity, so that the activation density may be reducible to < 1%. The photoswitching kinetics of the Dronpa mutant favored for PALMIRA, rsFastLime (Dronpa-V157G)[6] are somewhat different from those of mApple, but specific selection for variants with the desired kinetics or structure-guided design of mutants with altered photoswitching properties should be possible. While our laser scanning confocal bleach curves (**Fig. 1** in the main text) suggest that mApple is quite photostable under high intensity intermittent illumination, it is yet to be determined if constant illumination at the higher intensities required for PALMIRA will lead to a larger degree of irreversible photobleaching. Thus, we believe that mApple or future variants have the potential to be genetically encoded red FPs complementary to green Dronpa for PALMIRA.

References

1. Shaner, N.C. et al. Improved monomeric red, orange and yellow fluorescent proteins derived from Discosoma sp. red fluorescent protein. *Nat Biotechnol* **22**, 1567-1572 (2004).
2. Yarbrough, D., Wachter, R.M., Kallio, K., Matz, M.V. & Remington, S.J. Refined crystal structure of DsRed, a red fluorescent protein from coral, at 2.0-A resolution. *Proc Natl Acad Sci U S A* **98**, 462-467 (2001).
3. Verkhusha, V.V., Chudakov, D.M., Gurskaya, N.G., Lukyanov, S. & Lukyanov, K.A. Common Pathway for the Red Chromophore Formation in Fluorescent Proteins and Chromoproteins. *Chem Biol* **11**, 845-854 (2004).
4. Andresen, M. et al. Structure and mechanism of the reversible photoswitch of a fluorescent protein. *Proc Natl Acad Sci U S A* **102**, 13070-13074 (2005).
5. Andresen, M. et al. Structural basis for reversible photoswitching in Dronpa. *Proc Natl Acad Sci U S A* (2007).
6. Stiel, A.C. et al. 1.8 A bright-state structure of the reversibly switchable fluorescent protein Dronpa guides the generation of fast switching variants. *Biochem J* **402**, 35-42 (2007).
7. Egner, A. et al. Fluorescence nanoscopy in whole cells by asynchronous localization of photoswitching emitters. *Biophys J* **93**, 3285-3290 (2007).

Supplementary Note 2

Evolution of a photostable orange monomer. To determine whether the combination of Q64H and F99Y mutations could confer enhanced photostability on related fluorescent protein variants, we introduced these mutations into mRFP1 (ref. 1), the second-generation variant mCherry[2], and mApple (see main text). As with mOrange, the Q64H mutation alone did not lead to an increase in photostability of any of these variants (data not shown). However, the combination of Q64H and F99Y conferred an ~11-fold increase in photostability to mRFP1, making it as photostable as its successor, mCherry (data not shown). However, these mutations also had undesirable effects on maturation and folding efficiency of mRFP1, making the double mutant suboptimal compared with mCherry. Interestingly, the combination of Q64H and F99Y had no effect on the photostability of mCherry or mApple, suggesting that this combination of mutations specifically enhances photostability in mRFP1 variants possessing methionine at position 163. It is tempting to speculate that substitutions at 163 may inhibit photobleaching by the same mechanism as the Q64H + F99Y double mutation.

To determine if photobleaching was occurring through an oxidative mechanism, we measured bleaching curves for mOrange and mOrange2 before and after removing O_2 by equilibration of the bleaching chamber under N_2. Anoxia led to a dramatic increase in mOrange photobleaching half-time (approximately 25-fold, see **Fig. 1a** and **Table 1** in the main text), indicating that the primary mechanism for mOrange photobleaching under normoxic conditions is oxidative. Interestingly, anoxia had almost no effect on the photobleaching curve of mOrange2 (**Fig. 1d** in the main text), indicating that its primary bleaching mechanism is fundamentally different from that of mOrange and that the photostability-enhancing mutations almost completely suppress the oxidative bleaching pathway. However, anoxia did prevent the small amount of photoactivation observed for mOrange2 under normal conditions, indicating that this effect remains oxygen-dependent.

To confirm the fusion tolerance and targeting functionality of mOrange2 in a wide range of host protein chimeras, we have developed a series of 20 mOrange2 fusion constructs to both the C- and N-terminus of the fluorescent protein. In all cases, the localization patterns of the fusion proteins was similar to those that we have simultaneously or previously confirmed with avGFP fusions (mEGFP and mEmerald; data not shown) (see **Fig. 2** in the main text). Fusions of mOrange2 to histone H2B were observed not to hinder successful cell division as all phases of mitosis were present in cultures expressing this construct (**Fig. 2q-u** in the main text). mOrange2 also performed well as a fusion to the microtubule (+)-end binding protein, EB3 (**Fig. 2e** in the main text) where it could be observed tracing the path of growing microtubules in time-lapse image sequences. Thus, mOrange2 is expected to perform as well as highly validated fluorescent proteins such as mEGFP in fusion constructs.

In order to compare the targeting capabilities of mOrange2 to other fluorescent proteins in the orange spectral class, we constructed fusions of mKusabira Orange (mKO) and tdTomato to human a-tubulin and rat a-1 connexin-43 and imaged them in HeLa cells along with identical fusions to mOrange2 (**Fig. C** below). Because they are tightly packed in ordered tubulin filaments, fluorescent protein fusions to a-tubulin often do not localize properly if any degree of oligomeric character is present in the fluorescent protein or if the construct experiences steric hindrance due to the size and/or folding behavior of the fluorescent protein. Similarly, connexin-43 fusions are also sensitive to fluorescent protein structural parameters in localization experiments.

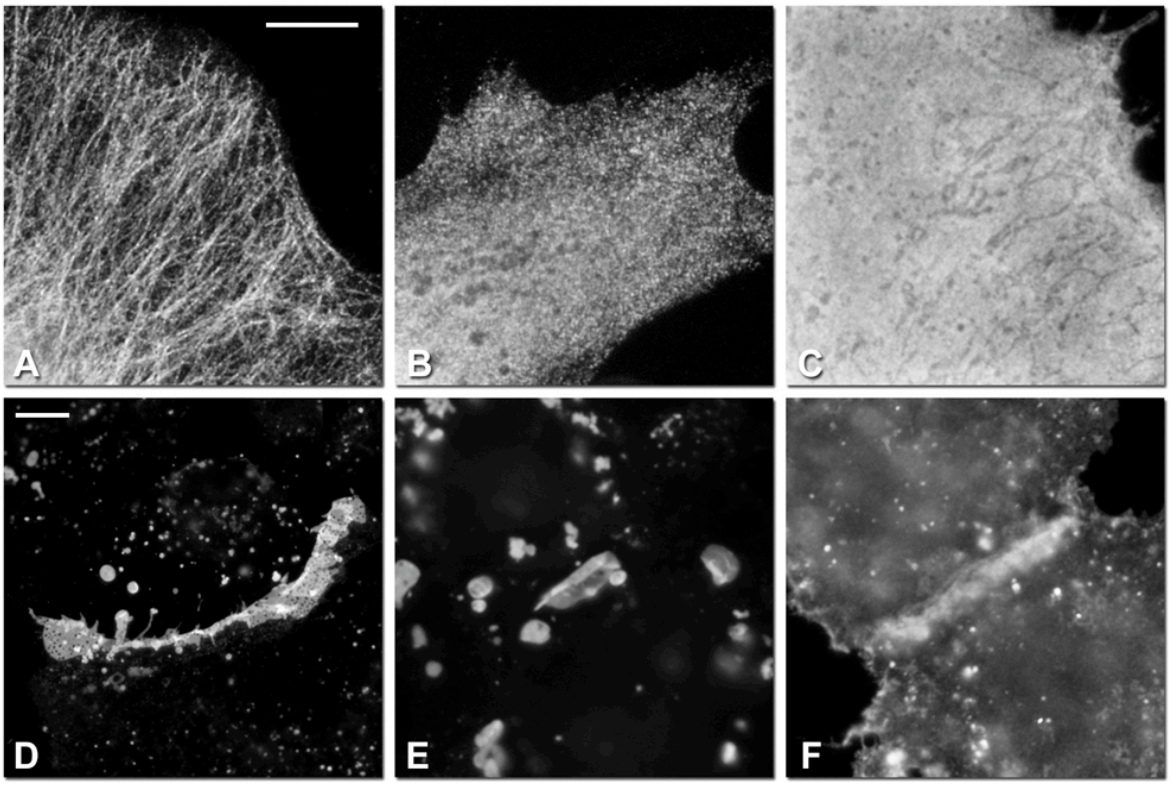

Figure C. Comparison of mOrange2, mKO, and tdTomato fusions in microtubules and gap junctions. (**a**–**c**) Widefield fluorescence images of HeLa cells expressing an identical human a-tubulin (C-terminus; 6-amino acid linker) localization construct fused to: (**a**) mOrange2; (**b**) mKO; (**c**) tdTomato. 100x magnification; Bar = 10 mm. (**d**–**f**) HeLa cells expressing an identical rat a-1 connexin-43 (N-terminus; 7-amino acid linker) localization construct fused to (**d**) mOrange2; (**e**) mKO; (**f**) tdTomato. 60x magnification; Bar = 10 mm.

Fusions of mOrange2 to a-tubulin localize as expected to produce discernable microtubule filaments (**Fig. Ca** above), but the same construct substituting mKO for mOrange2 exhibits punctate behavior that obscures the identification of any tendency to form filaments (**Fig. Cb** above). The tdTomato-a-tubulin fusion shows no evidence of localization and produces patterns reminiscent of whole-cell expression by the fluorescent protein without a fusion partner (note the dark outlines of mitochondria in the cytoplasm: **Fig. Cc** above). Fusions of mOrange2 with rat a-1 connexin-43 are assembled in the endoplasmic reticulum and traffic through the Golgi complex before being translocated to the plasma membrane and properly assembled into functional gap junctions (**Fig. Cd** above). In contrast, mKO fusions with connexin-43 produce extraordinarily large cytoplasmic vesicles and form less clearly defined and much smaller gap junctions (**Fig. Ce** above). tdTomato-connexin-43 fusions form aggregates in the cytoplasm accompanied by widespread labeling of the membrane with no apparent trafficking patterns through the endoplasmic reticulum and Golgi complex. In addition, the fusion does not form morphologically distinct gap junctions, but occasionally will produce regions of brighter fluorescence where plasma membranes of neighboring cells overlap (**Fig. Cf** above). In all other fusions tested, mKO performed as well as mOrange2 (data not shown), suggesting that most proteins will tolerate fusion to either protein.

References

1. Campbell, R.E. et al. A monomeric red fluorescent protein. *Proc Natl Acad Sci U S A* **99**, 7877-7882 (2002).
2. Shaner, N.C. et al. Improved monomeric red, orange and yellow fluorescent proteins derived from Discosoma sp. red fluorescent protein. *Nat Biotechnol* **22**, 1567-1572 (2004).

Supplementary Note 3

Reversible photoswitching assays. Our observation that our newly engineered photostable fluorescent protein variants exhibited varying degrees of reversible photoswitching led us to explore this phenomenon in other commonly used fluorescent proteins. To qualitatively measure this behavior, histone H2B fusions to each fluorescent protein were expressed and imaged in HeLa-S3 cells by widefield and laser scanning confocal microscopy (LSCM) (for instrumentation, see **Live cell imaging** and **LSCM live cell photobleaching** in **Supplementary Methods**). For both widefield and LSCM imaging, cells were exposed to constant illumination without neutral density filters (widefield) or with 25-100% laser power (LSCM) (corresponding to excitation intensities between 32 and 151 W/cm^2 for widefield and between 49 and 637 W/cm^2 (scan-averaged) for LSCM) until they had dimmed to between 75% and 50% initial fluorescence intensity. The cells were then allowed to recover in darkness for 1 to 2 minutes, after which time they were re-imaged. Any recovery of fluorescence could not be due to diffusion from non-illuminated regions, because the histone H2B fusions were confined within nuclei that were entirely within the bleached area. The percent recovery (*%REC*) of the peak initial fluorescence was calculated as:

$$\%REC = \frac{f_r - f_{bl}}{f_0 - f_{bl}}$$

where f_0 is the peak initial fluorescence, f_{bl} is the post-bleach fluorescence, and f_r is the post-dark recovery fluorescence. See **Fig. D** below for an example of the behavior of EGFP under widefield and confocal illumination. Results for a wide variety of FPs are reported in **Table A** below. While these data strongly suggest that reversible photoswitching is a common feature among fluorescent proteins, these data are not intended to be quantitative; further in-depth investigation of this phenomenon under a wider variety of experimental conditions will be necessary to fully characterize this effect and its possible implications in any given experiment.

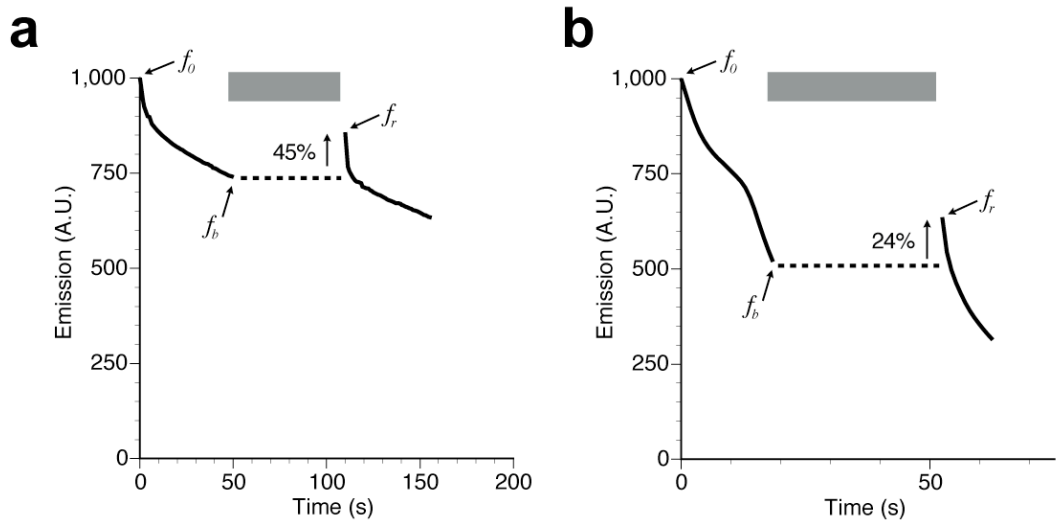

Figure D. Example of reversible photoswitching curves for mEGFP. For both (a) widefield and (b) confocal imaging, cells expressing histone H2B fused to mEGFP were exposed to constant illumination until measurably bleached, then the cells were then allowed to recover in darkness for approximately 1 minute (indicated by the grey bars), after which time they were re-imaged. The initial fluorescence value f_0, post-bleach fluorescence f_b, and post-recovery fluorescence f_r are indicated by the arrows. In this experiment, mEGFP exhibits 45% recovery during widefield imaging and 24% recovery during laser scanning confocal imaging. Note that photobleaching times have not been normalized for differences in excitation intensity.

Table A. Summary of reversible photoswitching data.

Protein[a]	**% recovery, widefield (excitation intensity)**[b]	**% recovery, confocal (excitation intensity)**[b]
TagRFP-T	13 (96 W/cm^2)	30 (181 W/cm^2)
TagRFP	4 (108 W/cm^2)	14 (181 W/cm^2)
mOrange2	6 (96 W/cm^2)	4.1 (181 W/cm^2)
mCherry	14 (151 W/cm^2)	4 (181 W/cm^2)
tdTomato	ND[c]	0 (181 W/cm^2)
mKO	4 (96 W/cm^2)	18 (181 W/cm^2)
mKate	0 (155 W/cm^2)	6.6 (181 W/cm^2)
mCerulean	113 (50 W/cm^2)	10 (230 W/cm^2)
mVenus	23 (32 W/cm^2)	47 (225 W/cm^2)
EYFP	9.8 (32 W/cm^2)	31 (225 W/cm^2)
Citrine	5.9 (32 W/cm^2)	38 (441 W/cm^2)
YPet	10 (32 W/cm^2)	24 (49 W/cm^2)
Topaz	16 (32 W/cm^2)	65 (225 W/cm^2)
mEGFP	45 (54 W/cm^2)	24 (637 W/cm^2)

[a] Fluorescent proteins fused to histone H2B and expressed in HeLa-S3 cells (see text above).

[b] Percent dark recovery of fluorescence after dimming to between 50 and 75% initial peak fluorescence, followed by 1 to 2 minutes darkness; see text above for complete description and **Figure D** above for representative mEGFP traces. Excitation intensity, as measured at the objective, is shown in parentheses (scan-averaged for LSCM).

[c] ND = not determined

To more precisely characterize the degree of reversible photoswitching in three representative proteins (TagRFP, TagRFP-T, and Cerulean), aqueous droplets of purified protein under oil were bleached on a microscope at ambient temperatures with xenon arc lamp illumination through a 540/25 filter (for TagRFP and TagRFP-T) or 420/20 nm filter (for Cerulean) without neutral density filters for short (~2 to 10s) or long (~2 to 10 min) intervals, and allowed to recover in the dark while fluorescence intensity was measured with 50ms exposures (**Fig. E** below). All three proteins were able to recover to nearly 100% after very short periods of bleaching, and to a lesser degree after longer periods. Once again, these data strongly indicate the need for further investigation of this phenomenon in all commonly used fluorescent proteins.

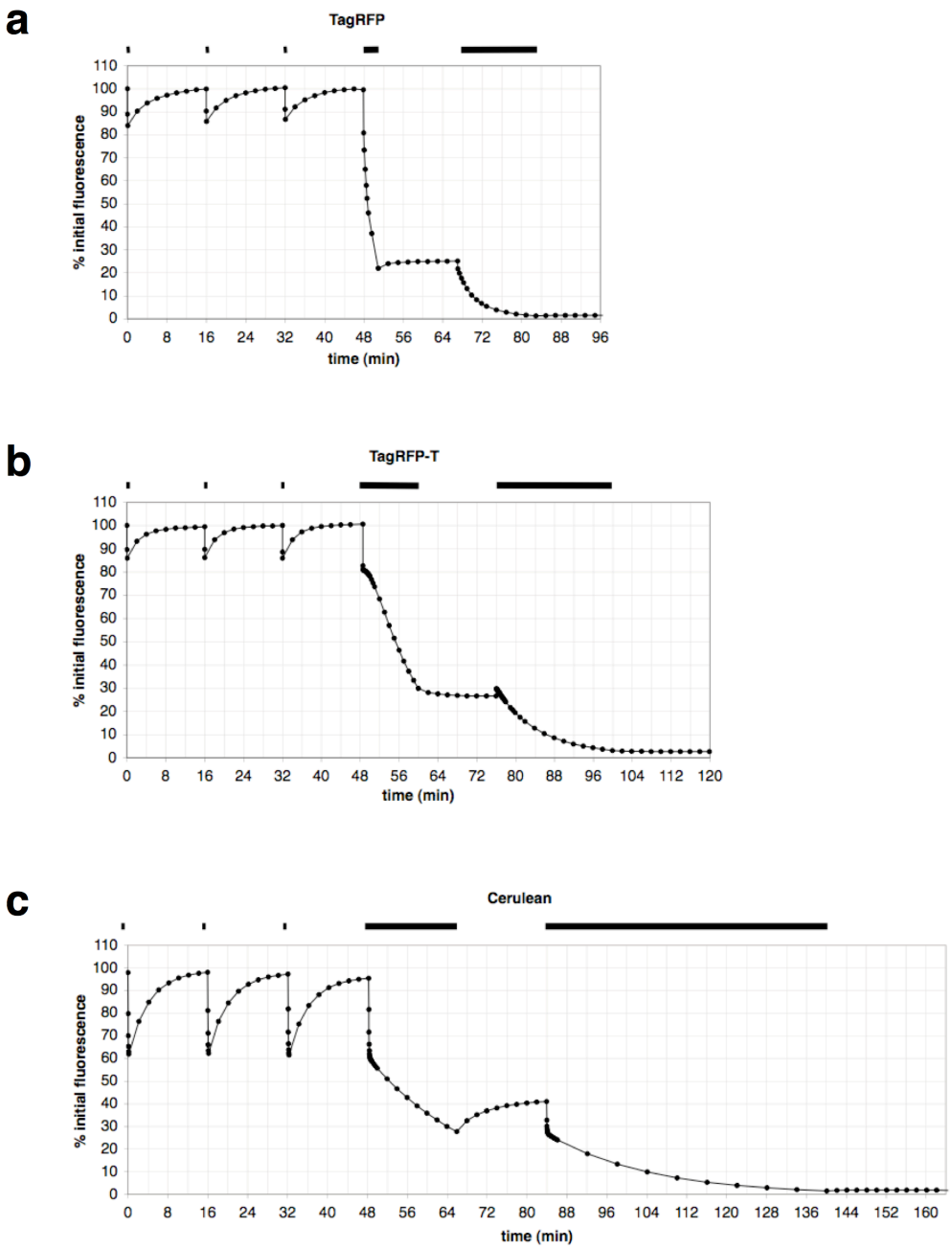

Figure E. Reversible photoswitching of TagRFP, TagRFP-T, and Cerulean during widefield microscopy. (a) A fraction of TagRFP fluorescence recovers after both short and sustained photobleaching. Purified TagRFP was bleached on a microscope at ambient temperatures with xenon arc lamp illumination through a 540/25 nm filter for short (~2s) or long intervals as indicated by the bars, and allowed to recover in the dark while fluorescence intensity was measured with 50ms exposures. (b) A fraction of TagRFP-T fluorescence recovers after short photobleaching, but not after sustained photobleaching. (c) Cerulean demonstrates fluorescence recovery after short (~10s) and sustained photobleaching through a 420/20 nm filter. Exposure intervals are indicated by bars. Note that photobleaching times are raw, and have not been adjusted for different illumination powers and the different extinction coefficients and quantum yields as is done to derive normalized photostability measurements.

Supplementary Methods

Primer list.

mFr-BamHI-F	CCTCGGATCCGATGGTGAGCAAGGGCGAGGAG
mFr-EcoRI-R	CCTCGAATTCTTACTTGTACAGCTCGTCCATGCC
mOr-T66Q-F	CTGTCCCCTCAGTTCGAGTACGGCTCCAAGGCC
mOr-T66Q-R	GGCCTTGGAGCCGTACTCGAACTGAGGGGACAG
mAp0.1-Q66M-F	CTGTCCCCTCAGTTCATGTACGGCTCCAAGGCC
mAp0.1-Q66M-R	GGCCTTGGAGCCGTACATGAACTGAGGGGACAG
mAp0.1-A217NNK-F	GGAACAGTACGAACGCNNKGAGGGCCGCCACTC
mAp0.1-A217NNK-R	GAGTGGCGGCCCTCMNNGCGTTCGTACTGTTCC
mAp0.1-M163HHK-F	CTGAAGGGCGAGATCAAGHHKAGGCTGAAGCTGAAGGAC
mAp0.1-M163HHK-R	GTCCTTCAGCTTCAGCCTKDDCTTGATCTCGCCCTTCAG
mAp0.2-69-73-F	GTACGGCTSCARGRBCTWCNTKAAGCACCCCGCCGACATCCCC
mAp0.2-69-73-R	GTGCTTMANGWAGVYCYTGSAGCCGTACATGAACTGAGGGGACAG
mAp0.2-105-8-F	GGCGGCNTKNTYHMCDHKHMCCAGGACTCCTCCCTGCAGGAC
mAp0.2-105-8-R	GTCCTGGKDMDHGKDRANMANGCCGCCGTCCTCGAAGTTC
mAp0.2-124NNK-F	GGCGTGTTCATCTACAAGGTGAAGNNKCGCGGCACCAACTTCCC
mAp0.2-124NNK-R	GGGAAGTTGGTGCCGCGMNNCTTCACCTTGTAGATGAACACGCC
mAp0.2-14-17-F	CATCATCAAGGAGTTCATGCGCYWKAAGGTGNNKATGGAGGGCTCCGTGAAC
mAp0.2-14-17-R	GTTCACGGAGCCCTCCATMNNCACCTTMWRGCGCATGAACTCCTTGATGATG
mAp0.2-V73X-F	GGCCTACNNKAAGCACCCCGCCGACATCC
mAp0.2-V73X-R	CGGGGTGCTTMNNGTAGGCCTTGGAGCCGTACATGAACTG
mAp0.2-195-9-F	GCCTACATCNTKGACRBKAAGNYKGACATCACCTCCCACAACGAGGAC
mAp0.2-195-9-R	GGTGATGTCMRNCTTMVYGTCMANGATGTAGGCGCCGGGCAG
mAp0.3-M97NTK-F	CTTCAAGTGGGAGCGCGTGNTKAACTTCGAGGACGGCGGC
mAp0.3-M97NTK-R	GCCGCCGTCCTCGAAGTTMANCACGCGCTCCCACTTGAAG
mAp0.4-K163QH-F	GCCCTGAAGAGCGAGATCAAGCASAGGCTGAAGCTGAAGGACG
mAp0.4-K163QH-R	CGTCCTTCAGCTTCAGCCTSTGCTTGATCTCGCTCTTCAGGGC
mAp0.4-S159TN-F	GAGGACGGCGCCCTGAAGAMCGAGATCAAGAAGAGGCTGAAG
mAp0.4-S159TN-R	CTTCAGCCTCTTCTTGATCTCGKTCTTCAGGGCGCCGTCCTC
mAp0.4-63-4-F	GCCTGGGACATCCTGTCCASCSWGTTCATGTACGGCTCCAAGGCC
mAp0.4-63-4-R	GGCCTTGGAGCCGTACATGAACWSGSTGGACAGGATGTCCCAGGC
mAp0.4-70+73-F	CAGTTCATGTACGGCTCCMRGGYCTACVHKAAGCACCCAGCCGACATC
mAp0.4-70+73-R	GATGTCGGCTGGGTGCTTMDBGTAGRCCYKGGAGCCGTACATGAACTG
mAp0.4-145-7-F	GAAGACCATGGGCTGGGAGSCCAVCAVCGAGCGGATGTACCCCGAG
mAp0.4-145-7-R	CTCGGGGTACATCCGCTCGBTGBTGGSCTCCCAGCCCATGGTCTTC
mAp0.4-161NTK-F	CGCCCTGAAGAGCGAGNTKAAGAAGAGGCTGAAGCTGAAG
mAp0.4-161NTK-R	CTTCAGCTTCAGCCTCTTCTTMANCTCGCTCTTCAGGGCG
mAp-mCh-Q64H-F	CTGGGACATCCTGTCCCCTCACTTCATGTACGGCTCCAAGGCC
mAp-mCh-Q64H-R	GGCCTTGGAGCCGTACATGAAGTGAGGGGACAGGATGTCCCAG
mOr-M163K-F	AAGGGCGAGATCAAGAAGAGGCTGAAGCTGAAG
mOr-M163K-R	CTTCAGCTTCAGCCTCTTCTTGATCTCGCCCTT
mOr-Q64H-F	CTGGGACATCCTGTCCCCTCACTTCACCTACGGCTCCAAGGC
mOr-Q64H-R	GCCTTGGAGCCGTAGGTGAAGTGAGGGGACAGGATGTCCCAG
mOr-64YAK-F	CTGGGACATCCTGTCCCCTYAKTTCACCTACGGCTCCAAGGCC
mOr-64YAK-R	GGCCTTGGAGCCGTAGGTGAAMTRAGGGGACAGGATGTCCCAG
mOr-97-9WWK-YWC-F	GGCTTCAAGTGGGAGCGCGTGWWKAACYWCGAGGACGGCGGCGTGGTG
mOr-97-9WWK-YWC-R	CACCACGCCGCCGTCCTCGWRGTTMWWCACGCGCTCCCACTTGAAGCC
mOr-M163HHK-F	CTGAAGGGCGAGATCAAGHHKAGGCTGAAGCTGAAGGAC
mOr-M163HHK-R	GTCCTTCAGCTTCAGCCTKDDCTTGATCTCGCCCTTCAG
mOr-175-7DYK-NTK-F	GACGGCGGCCACTACACCDYKGAGNTKAAGACCACCTACAAGGCCAAG
mOr-175-7DYK-NTK-R	CTTGGCCTTGTAGGTGGTCTTMANCTCMRHGGTGTAGTGGCCGCCGTC
mOr-97NTK-99YWC-F	GGCTTCAAGTGGGAGCGCGTGNTKAACYWCGAGGACGGCGGCGTGGTG

mOr-97NTK-99YWC-R	CACCACGCCGCCGTCCTCGWRGTTMANCACGCGCTCCCACTTGAAGCC
TagRFP-BamHI-F	AAGGATCCGATGGTGTCTAAGGGCGAAGAGC
TagRFP-BsrGI-R	CCTGTACAGCTCGTCCATGCCATTAAGTTTGTGCCCCAGTTTGCTAGG
TagRFP-158-F	GGCCTGGAAGGCAGANNSGACATGGCCCTGAA
TagRFP-158-R	TTCAGGGCCATGTCSNNTCTGCCTTCCAGGCC
TagRFP-199-F	TATGTGGACCACAGANNSGAAAGAATCAAGGAG
TagRFP-199-R	CTCCTTGATTCTTTCSNNTCTGTGGTCCACATA
mOr2-TagRFP-T-AgeI-F	CCTCACCGGTCGCCACCATGGTGAGCAAGGGCGAGGAG
mOr2-TagRFP-T-BspEI-R	CCTCTCCGGACTTGTACAGCTCGTCCATGCC
mOr2-TagRFP-T-NotI-R	CCTCGCGGCCGCTTTACTTGTACAGCTCGTCCATGCC

Mass spectrometry analysis. Parallel samples of purified mOrange were prepared without bleaching and with 60 minutes bleaching on the solar simulator, and dialyzed into 200 mM ammonium bicarbonate pH 8.5. Samples were then digested with LysC (Wako Biochemicals) which cuts at the C-terminal side of lysine, or AspN (Roche Diagnostics) which cuts at the N-terminal side of aspartic acid. For the LysC digests, protein was denatured in 6 M guanidinium HCl with incubation in a 72° C water bath for 2 minutes, followed by addition of LysC enzyme at a 30:1 protein to enzyme ratio, and incubation for 18 hours at 36° C. For the AspN digests, protein was denatured in 8 M urea with incubation in a 90° C water bath for 2 minutes, followed by addition of AspN enzyme at a 50:1 protein to enzyme ratio, an incubation for 18 hours at 36° C. Digested peptides were desalted with a C18 ZipTip (Millipore) to prepare the sample for matrix-assisted laser desorption/ionization (MALDI) mass spectrometry. The MALDI matrix used was α-cyanohydroxycinnamic acid (Fluka). Mass spectra were collected on an Voyager-DE STR MALDI-TOF (Applied Biosystems) using default tuning parameters.

Mammalian expression vectors. All mOrange2 and TagRFP-T expression vectors were constructed using C1 and N1 (Clontech-style) cloning vectors. The fluorescent protein was amplified with a 5' primer encoding an AgeI site and a 3' primer encoding either a BspEI (C1) or NotI (N1) site (see **Primer list**, above). The purified and digested PCR products were ligated into similarly digested pEGFP-C1 and pEGFP-N1 (Clontech) cloning vector backbones. To generate fusion vectors, the appropriate cloning vector and an EGFP fusion vector were digested, either sequentially or doubly, with the appropriate enzymes and ligated together after gel purification. Thus, to prepare N-terminal fusions, the following digests were performed: human non-muscle α-actinin, *Eco*RI and *Not*I (vector source, Tom Keller, FSU); human cytochrome C oxidase subunit VIII, *Bam*HI and *Not*I (mitochondria, Clontech); rat α-1 connexin-43 and β-2 connexin-26, *Eco*RI and *Bam*HI (Matthias Falk, Lehigh University); human histone H2B, *Bam*HI and *Not*I (George Patterson, NIH); N-terminal 81 amino acids of human β-1,4-galactosyltransferase, *Bam*HI and *Not*I (Golgi, Clontech); human microtubule-associated protein EB3, *Bam*HI and *Not*I (Lynne Cassimeris, Lehigh University); human vimentin, *Bam*HI and *Not*I (Robert Goldman, Northwestern University); human keratin 18, *Eco*RI and *Not*I (Open Biosystems); chicken paxillin, *Eco*RI and *Not*I (Alan Horwitz, University of Virginia); rat lysosomal membrane glycoprotein 1, *Age*I and *Nhe*I (George Patterson, NIH). To prepare C-terminal fusions, the following digests were performed: human β-actin, *Nhe*I and *Bgl*II (Clontech); human α-tubulin, *Nhe*I and *Bgl*II (Clontech); human light chain clathrin, *Nhe*I and *Bgl*II (George

Patterson, NIH); human lamin B1, *Nhe*I and *Bgl*II (George Patterson, NIH); human fibrillarin, *Age*I and *Bgl*II (Evrogen); human vinculin, *Nhe*I and *Eco*RI (Open Biosystems); peroximal targeting signal 1 (PTS1 - peroxisomes), *Age*I and *Bsp*EI (Clontech); human RhoB GTPase with an N-terminal c-Myc epitope tag (endosomes), *Age*I and *Bsp*EI (Clontech). DNA for mammalian transfection was prepared using the Plasmid Maxi kit (Qiagen).

Live cell imaging. HeLa epithelial (CCL-2, ATCC) and Grey fox lung fibroblast (CCL-168, ATCC) cells were grown in a 50:50 mixture of DMEM and Ham's F12 with 12.5% Cosmic calf serum (HyClone) and transfected with Effectene (Qiagen). Imaging was performed in Delta-T culture chambers (Bioptechs) under a humidified atmosphere of 5% CO_2 in air. Fluorescence images in widefield mode were gathered using a TE-2000 inverted microscope (Nikon) equipped with QuantaMax™ filters (Omega) and a Cascade II camera (Photometrics) or an IX71 microscope (Olympus) equipped with BrightLine™ filters (Semrock) and a ImagEM™ camera (Hamamatsu). Laser scanning confocal microscopy was performed on C1Si (Nikon) and FV1000 (Olympus), both equipped with helium-neon and diode lasers and proprietary filter sets to match fluorophore emission spectral profiles. Spinning disk confocal microscopy was performed on a DSU-IX81 microscope (Olympus) equipped with a Lumen 200 illuminator (Prior), Semrock filters, 10-position filter wheels driven by a Lambda 10-3 controller (Sutter), and a 9100-12 EMCCD camera (Hamamatsu). Cell cultures expressing fluorescent protein fusions were fixed after imaging in 2% paraformaldehyde (EMS) and washed several times in PBS containing 0.05 M glycine before mounting with a polyvinyl alcohol-based medium. Morphological features in all fusion constructs were confirmed by imaging fixed cell preparations on coverslips using an 80i upright microscope (Nikon) and ET-DsRed filter set (#4900; Chroma) coupled to an Orca ER (Hamamatsu) or a CoolSNAP™ HQ^2 (Photometrics) camera.

Laser scanning confocal microscopy live cell photobleaching. Laser scanning confocal microscopy (LSCM) photobleaching experiments were conducted with N-terminal fusions of the appropriate fluorescent protein to human histone H2B (6-residue linker) to confine fluorescence to the nucleus in order to closely approximate the dimensions of aqueous droplets of purified FPs used in widefield measurements. HeLa-S3 cells (average nucleus diameter = 17μm) were transfected with the H2B construct using Effectene (Qiagen) and maintained in a 5% CO_2 in Delta-T imaging chambers (Bioptechs) for at least 36 hours prior to imaging. The chambers were transferred to a stage adapter (Bioptechs), imaged at low magnification to ensure cell viability, and then photobleaching using a 40x oil immersion objective (Olympus UPlan Apo, NA = 1.00). Laser lines (543 nm, He-Ne and 488 nm, argon-ion) were adjusted to an output power of 50 μW, measured with a FieldMaxII-TO (Coherent) power meter equipped with a high-sensitivity silicon/germanium optical sensor (OP-2Vis, Coherent). The instrument (FV300, Olympus) was set to a zoom of 4X, a region of interest of 341.2 μm^2 (108 x 108 pixels), a photomultiplier voltage of 650 V, and an offset of 9% with a scan time of 0.181 seconds

per frame. Nuclei having approximately the same dimensions and intensity under the fixed instrument settings were chosen for photobleaching assays. Fluorescence using the 543 laser was recorded with a 570 nm dichromatic mirror and 656 nm longpass barrier filter, whereas emission using the 488 laser was directly reflected by a mirror through a 510 nm longpass barrier filter. The photobleaching half-times for LSCM imaging were calculated as the time required to reduce the scan-averaged emission rate to 50% from an initial emission rate of 1000 photons/s per fluorescent protein chromophore. Briefly, the average photon flux (photons/(s x m^2)) over the scanned area of interest was calculated thus:

$$\Phi = \frac{P}{EA} = \frac{P\lambda}{hcA}$$

where P is the output power of the laser measured at the objective in Joules/sec, A is the scanned area in m^2, and $E = \frac{hc}{\lambda}$ is the energy of a photon in Joules at the laser wavelength (either 543 nm or 488 nm). The optical cross section (in cm^2) of a fluorescent protein chromophore is given by:

$$\sigma(\lambda) = \frac{(1000\text{cm}^3/\text{L})(\ln 10)\varepsilon(\lambda)}{6.023 \times 10^{23}/\text{mole}}$$

where $\varepsilon(\lambda)$ is the extinction coefficient of the fluorescent protein at the laser wavelength in M^{-1} x cm^{-1}. And so the scan-average excitation rate per fluorescent molecule is given by:

$$X = \Phi\sigma(\lambda)$$

and so the time to bleach from an initial scan-averaged rate of 1000 photons/s to 500 photons/s is:

$$t_{1/2} = \frac{t_{raw} XQ}{1000\text{photons/s}}$$

where t_{raw} is the measured photobleaching half-time and Q is the fluorescent protein quantum yield. To produce full bleaching curves, we simply scale the raw time coordinates by the factor $\frac{XQ}{1000\text{photons/s}}$ and normalize the intensity coordinate to 1000 photons/s initial emission rate.